JOURNAL OF GUIDANCE, CONTROL, AND DYNAMICS
Vol. 29, No. 4, July–August 2006

Adaptive Output Feedback Control for Spacecraft Rendezvous and Docking Under Measurement Uncertainty

Puneet Singla*
Texas A&M University, College Station, Texas 77843
Kamesh Subbarao†
University of Texas, Arlington, Texas 76019
and
John L. Junkins‡
Texas A&M University, College Station, Texas 77843

An output feedback structured model reference adaptive control law has been developed for spacecraft rendezvous and docking problems. The effect of bounded output errors on controller performance is studied in detail. Output errors can represent an aggregation of sensor calibration errors, systematic bias, or some stochastic disturbances present in any real sensor measurements or state estimates. The performance of the control laws for stable, bounded tracking of the relative position and attitude trajectories is evaluated, considering unmodeled external as well as parametric disturbances and realistic position and attitude measurement errors. Essential ideas and results from computer simulations are presented to illustrate the performance of the algorithm developed in the paper.

Introduction

AUTONOMOUS rendezvous and docking are essential for future autonomous space transportation missions such as International Space Station supply and repair and automated inspection, servicing, and assembly of space systems. Autonomous proximity operations are required for a large number of future mission concepts but cannot be achieved routinely at present. For the docking of two spacecraft, highly precise and robust position and attitude control is required, which further requires precise measurements of the relative position and attitude of docking spacecraft. These requirements have driven the identification, development, and evaluation of several relative navigation sensors, such as VGS (video guidance sensor) and global positioning system[1−3] (GPS). Traditional relative navigation and guidance technology is based upon the use of GPS and various types of VGS. Although both technologies have been used successfully in many missions, they suffer from some serious shortcomings that limit their use in future missions. The GPS measurements are suspectable to multipath effects whereby a signal arrives at a receiver via multiple paths due to reflection and diffraction of the electromagnetic waves. Due to multiple reflections the multipath signal takes longer than the direct signal and, hence, causes degradation in navigation accuracy. Multipath effects are bound to exist in rendezvous and docking operations, because the chaser spacecraft and the target spacecraft GPS antennas are surrounded by many large metallic structures. On the other hand, VGS technology suffers from difficulties that include often inadequate spatial accuracy, slow frame rates, image processing computational burden, difficulties with accommodating lighting variations, and occasional failure of pattern recognition methods. An additional set of challenges arise due to wide variations in the depth of field (range) during relative motion of two spacecraft.

In the past decade, there have been many significant developments in the fields of solid-state electronics and photonics. These advances have further led to the growth of relative guidance and navigation sensor technologies such as light detection and ranging[4,5] (LIDAR), laser dynamics range imager[6,7] (LDRI), and optical sensors combined with structured active light sources. These advances have tried to address the many well-known shortcomings of the GPS and VGS technologies. Both LIDAR and LDRI use the time-of-flight calculations of the pulsed laser beam scattered back from the target on the system̀s detector to determine the range between the chaser spacecraft and the target spacecraft. The main difference between LIDAR and LDRI technologies is that LIDAR is based upon scanning laser radar,[4] whereas LDRI is a scannerless imaging laser radar that works by illuminating the scene with laser light and demodulating the captured signal via an array of detectors.[7] Although the use of LIDAR or LDRI would provide useful range information between the chaser spacecraft and the target spacecraft, along with video image information, at the same time issues such as power, mass, and volume of every lidar system, especially those targeted for space applications, need to be addressed.

In Refs. 8–11, a new kind of optical sensor combined with structured active light sources (beacons) is discussed as a way to achieve a selective or "intelligent" vision-based relative navigation solution. This is accomplished by fixing several light emitting diodes, called beacons, to a target frame (vehicle), and an optical sensor on a chaser frame (vehicle). The diodes emit structured light modulated with a known waveform and by filtering the received energy, ambient energy is ignored. This new optical sensor works analogously to radar and addresses many issues related to relative navigation and guidance. Any of the sensors discussed can form the basis for generating accurate relative position and attitude measurements for the problem studied in this paper. However, reliability, power, weight, accuracy, and cost of the sensors for the space missions determine the suitability of a sensor for a specific space mission.

Various navigation sensors, as discussed, are used to determine the target spacecraft's best estimated location and orientation state and then feed the estimated relative state information to an automated rendezvous and docking operations controller. Therefore, beside accurate sensing, autonomous spacecraft rendezvous and docking require very precise translational and rotational maneuvers. These requirements frequently necessitate the use of nonlinear spacecraft dynamic models for control system design. We will consider

Presented as Paper 2003-103 at the AAS/AIAA 13th Space Flight Mechanics Meeting, Ponce, Puerto Rico, 9–13 February 2003; received 2 May 2005; accepted for publication 19 September 2005.

*Graduate Assistant Research, Department of Aerospace Engineering; puneet@tamu.edu. Student Member AIAA.

†Assistant Professor, Department of Mechanical and Aerospace Engineering; subbarao@mae.uta.edu. Member AIAA.

‡Distinguished Professor, George Eppright Chair, Department of Aerospace Engineering; junkins@tamu.edu. Fellow AIAA.

a general asymmetric spacecraft containing three momentum wheels for attitude maneuvers, variable thrusters for translational maneuvers, and the nonlinear Clohessy–Wiltshire[12] equations to model the relative translation motion of the chaser spacecraft. The attitude motion of spacecraft will be represented by modified Euler equations for nonlinear relative angular velocity evolution and attitude parameter kinematic equations. Although Clohessy–Wiltshire equations and Euler's equations represent a near-exact dynamical model, for control design purposes, complications may arise from uncertain spacecraft inertia and mass properties, which can change due to fuel consumption, solar array deployment, payload variation, etc. Furthermore, stability robustness in presence of model errors, measurement errors, and disturbances is a primary consideration for design of any autonomous control system.

To address the problems mentioned, a structured model reference adaptive control law[13,14] has been developed for the relative sensing-based spacecraft rendezvous and docking problem. The adaptive control law formulation normally requires full state measurements, which requires, for example, additional sensors on board such as rate gyros to measure the angular velocity of the spacecraft. To avoid the need for additional sensors (beyond the relative navigation sensors), the velocity level states can be "measured" (estimated) by effectively differentiating the position measurements,[15–17] although care must be taken due to the usual difficulties associated with differentiation of noisy signals. Crassidis et al. have developed an optimal and efficient noniterative algorithm for attitude and position determination from line-of-sight observations.[18] This algorithm makes use of high measurement rates (≈100 Hz) of vision sensors to estimate angular velocities and linear velocities to propagate a kinematic model. However, the approach was based upon the assumption that the separation principle for this class of nonlinear systems holds (it was not explicitly proved). Further, the velocity estimates were known to be susceptible to high measurement noise. In this paper, we use a purely geometric method[19] of position and attitude determination from line-of-sight observations, which, as is shown in subsequent sections, allows us to decouple the controller design from the observer design. In lieu of designing a conventional Kalman filterlike estimator to estimate velocity, an alternate approach had been used in Refs. [14, 20, 21] which utilizes a filter based on the passivity properties of the spacecraft translational and attitude dynamics to generate the pseudo-velocity-like signals. Although this filter-based approach effectively unifies observer and controller design methodology, this formulation still suffers from the assumption that perfect (error-free) position level state data are available to the filter as well as the controller for feedback, which is generally not true. In a realistic scenario, the presence of measurement errors makes it hard to conclude asymptotic stability of the controller. In this paper, another important step is taken by removing the assumption of perfect measurement of data and a realistic problem is considered where position measurement errors are accounted for.

Both the observer and the adaptive control formulations in this paper are based upon Lyapunov's direct stability theorem and impose exact kinematic equations at velocity level while taking care of model uncertainties and disturbances at acceleration level. An important contribution of the paper is explicit consideration of measurement errors and observer design in a nonlinear adaptive control setting. Stability analysis in the presence of noise/sensor errors provides us with a fundamental theoretical framework to tie together state estimation with controller design, which is missing in all the existing literature on nonlinear adaptive control.

The structure of this paper is as follows. First, the dynamical models for relative translational and rotational motion are set forth, followed by the partial state feedback adaptive controller design for translation and rotation motion. Then the effect of measurement noise on the performance of the controller is discussed. Finally, the controllers designed in this paper are tested using a simulated rendezvous and docking maneuver.

Equations of Motion

In this section, the model we adopt for nonlinear spacecraft dynamics, is set forth, which includes relative orbit dynamics, relative attitude kinematics, and rotational dynamics using momentum transfer torque actuation with three momentum wheels. This model is described in order to be specific in the further developments contained in this paper.

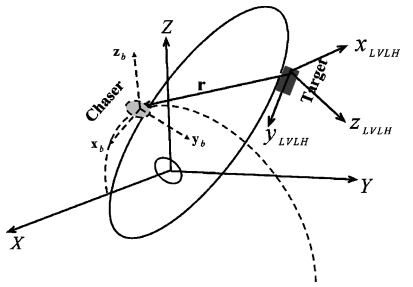

Fig. 1 LVLH and body frame.

Coordinate System

The relevant coordinate systems are 1) the local-vertical–local-horizontal[22] (LVLH) reference frame centered on the target space vehicle and 2) the orthogonal body frame fixed in the center of mass of the chaser spacecraft and centered at the chaser spacecraft, as shown in Fig. 1. The LVLH reference frame is attached to the center of mass of the target space vehicle with X-axis pointing radially outward from its orbit, Y-axis perpendicular to X along its direction of motion, and Z completing the right-handed coordinate system. Usually in rendezvous and docking problems, the trajectory of the target spacecraft is described in the LVLH coordinate system, and this frame is taken as the reference target trajectory for the chaser spacecraft.

Relative Motion Dynamics

The chaser motion relative to the target spacecraft in the LVLH frame is described by the fully nonlinear Clohessy–Wiltshire equations, given as follows[22]:

$$\ddot{x} - 2\dot{\theta}\dot{y} - \ddot{\theta}y - \dot{\theta}^2 x - 2\left(\mu/r_c^3\right)x = -\mu(r_c + x)/\rho^{\frac{3}{2}} + \mu/r_c^2 - 2\left(\mu/r_c^3\right)x + F_x/m$$

$$\ddot{y} + 2\dot{\theta}\dot{x} + \ddot{\theta}x - \dot{\theta}^2 y + \left(\mu/r_c^3\right)y = -\mu y/\rho^{\frac{3}{2}} + \left(\mu/r_c^3\right)y + F_y/m$$

$$\ddot{z} + \left(\mu/r_c^3\right)z = -\mu z/\rho^{\frac{3}{2}} + \left(\mu/r_c^3\right)z + F_z/m$$

$$\ddot{r}_c = r_c\dot{\theta}^2 - \mu/r_c^2, \qquad \ddot{\theta} = -2(\dot{r}_c\dot{\theta}/r_c)$$

$$\rho = \sqrt{(r_c + x)^2 + y^2 + z^2} \tag{1}$$

where x, y, z represent the relative position of chaser w.r.t. target, r_c and ρ refer to the scalar radius of the target and chaser from the center of the Earth, respectively, θ represents the latitude angle of the target, and μ is the gravitational parameters. F_x, F_y, and F_z are the control forces and m is the mass of chaser spacecraft. These equations amount to the classical nonlinear Encke[22] relative motion differential equations of the chaser vehicle written in the rotating LVLH coordinate system, centered on the target vehicle.

Attitude Dynamics

We introduce three reference frames, $\mathcal{N}$, $\mathcal{B}$, and $\mathcal{R}$, in this context to describe the relative rotational motion of the chaser spacecraft. The reference frame $\mathcal{N}$ corresponds to the inertial frame fixed to the center of the earth, whereas reference frames $\mathcal{B}$ and $\mathcal{R}$ denote the body-fixed and orbit-fixed LVLH reference axes. Further, the modified Rodrigues parameters (MRP) parameters[22] corresponding to the orientation of LVLH frame $\mathcal{R}$ with respect to inertial frame $\mathcal{N}$ are denoted by σ_r, whereas those corresponding to the orientation

of body frame $\mathcal{B}$ with respect to inertial frame $\mathcal{N}$ are denoted by σ. The triad of unit vectors in these three frames can be related by the following vectrix projection relationships:

$$\hat{\boldsymbol{b}} = \boldsymbol{C}(\boldsymbol{\sigma})\hat{\boldsymbol{n}}, \qquad \hat{\boldsymbol{r}} = \boldsymbol{C}(\boldsymbol{\sigma}_r)\hat{\boldsymbol{n}} \tag{2}$$

$$\hat{\boldsymbol{b}} = \boldsymbol{C}(\boldsymbol{e})\hat{\boldsymbol{r}}, \qquad \boldsymbol{C}(\boldsymbol{e}) = \boldsymbol{C}(\boldsymbol{\sigma})\boldsymbol{C}^T(\boldsymbol{\sigma}_r) \tag{3}$$

where $\boldsymbol{e}$ refers to the attitude tracking error MRP that parameterizes the rotational displacement error between the body frame and the LVLH frame. Notice, in general $\boldsymbol{e} \neq \boldsymbol{\sigma} - \boldsymbol{\sigma}_r$, although $\boldsymbol{e} \to 0 \Rightarrow \boldsymbol{\sigma} \to \boldsymbol{\sigma}_r$. The attitude matrix $\boldsymbol{C}(\boldsymbol{\sigma})$, in terms of the MRP, can be written as[22]

$$\boldsymbol{C}(\boldsymbol{\sigma}) = \boldsymbol{I} - 4[(1 - \boldsymbol{\sigma}^T\boldsymbol{\sigma})/(1 + \boldsymbol{\sigma}^T\boldsymbol{\sigma})^2][\tilde{\boldsymbol{\sigma}}] + [8/(1 + \boldsymbol{\sigma}^T\boldsymbol{\sigma})^2][\tilde{\boldsymbol{\sigma}}]^2 \tag{4}$$

The angular velocity error vector in the body frame can be represented as

$$\boldsymbol{\delta\omega} = \boldsymbol{\omega} - \boldsymbol{\eta}, \qquad \boldsymbol{\eta} = \boldsymbol{C}(\boldsymbol{e})\boldsymbol{\omega}_r \tag{5}$$

where $\boldsymbol{\omega} \in \Re^3$ represents the angular velocity of the chaser with components in the chaser vehicle body frame. Further, making use of the transport theorem,[22] we can rewrite the governing differential equations in terms of error angular rate and error MRP as follows[23,24]:

$$\dot{\boldsymbol{e}} = \tfrac{1}{4}\boldsymbol{J}(\boldsymbol{e})\boldsymbol{\delta\omega} \tag{6}$$

$$\boldsymbol{I}\dot{\boldsymbol{\delta\omega}} = -[\tilde{\boldsymbol{\omega}}]\boldsymbol{I}\boldsymbol{\omega} - \boldsymbol{A}\dot{\boldsymbol{\Omega}} - [\tilde{\boldsymbol{\omega}}]\boldsymbol{A}\boldsymbol{\Omega} + \boldsymbol{d} - \boldsymbol{I}[\boldsymbol{C}(\boldsymbol{e})\dot{\boldsymbol{\omega}}_r - [\tilde{\boldsymbol{\omega}}]\boldsymbol{\eta}] \tag{7}$$

where $\boldsymbol{I} \in \Re^{3\times 3}$ and $\boldsymbol{A} \in \Re^{3\times 3}$ represent the spacecraft and momentum wheel inertia matrices, respectively, and $\boldsymbol{\Omega} \in \Re^3$ represents the momentum wheel angular rate. $\boldsymbol{d} \in \Re^3$ is the next external disturbance torque affecting the relative attitude dynamics. We note that the momentum exchange terms (second, third, and last terms of Eq. (7)) constitute an effective torque that can be controlled through $\boldsymbol{\Omega}(t)$. The external disturbance torque in Eq. (7) can also be compensated for since the disturbance is matched[25] by the control input. $[\tilde{\boldsymbol{\omega}}]$ is the skew-symmetric matrix that represents the cross product of two vectors and can be written as

$$[\tilde{\boldsymbol{\omega}}] = \begin{bmatrix} 0 & -\omega_3 & \omega_2 \\ \omega_3 & 0 & -\omega_1 \\ -\omega_2 & \omega_1 & 0 \end{bmatrix} \tag{8}$$

Finally, the kinematic operator $\boldsymbol{J}(\boldsymbol{e})$ in Eq. (6) can be written as

$$\boldsymbol{J} = (1 - \boldsymbol{e}^T\boldsymbol{e})\boldsymbol{I}_{3\times 3} + 2[\tilde{\boldsymbol{e}}] + 2\boldsymbol{e}\boldsymbol{e}^T \tag{9}$$

Adaptive Control Law Formulation

In this section, the velocity-free adaptive control law is derived for translation and rotational motion maneuvers, using a Lyapunov direct stability theorem. This control law is derived along the same lines outlined in Refs. 20, 24. The novel feature of the control law developed in this paper is that it explicitly accounts for the uncertainties present in the state vector measurements (relative position and attitude).

Adaptive Control Formulation for Relative Translation Motion

In this section, we seek to design an adaptive feedback control law for the system described by Eq. (1) to track a given reference trajectory specified by $\boldsymbol{x}_r$. It should be noticed that Eq. (1) can be rewritten in the following form:

$$\dot{\boldsymbol{x}}_1 = \boldsymbol{x}_2, \qquad m\dot{\boldsymbol{x}}_2 = m\boldsymbol{A}_1\boldsymbol{x}_1 + m\boldsymbol{A}_2\boldsymbol{x}_2 + m\boldsymbol{g}(\boldsymbol{x}_1) + \boldsymbol{F} \tag{10}$$

where $\boldsymbol{x}_1 = [x\ \ y\ \ z]^T$ and $\boldsymbol{x}_2 = [\dot{x}\ \ \dot{y}\ \ \dot{z}]^T$ refer to relative position and velocity variables. The matrices $\boldsymbol{A}_1, \boldsymbol{A}_2$ and vector $\boldsymbol{g}$ can be constructed as follows:

$$\boldsymbol{A}_1 = \begin{bmatrix} \dot{\theta}^2 + 2\left(\mu/r_c^3\right) & \ddot{\theta} & 0 \\ -\ddot{\theta} & \dot{\theta}^2 - \mu/r_c^3 & 0 \\ 0 & & 0 \end{bmatrix} \tag{11}$$

$$\boldsymbol{A}_2 = \begin{bmatrix} 0 & 2\dot{\theta} & 0 \\ -2\dot{\theta} & 0 & 0 \\ 0 & 0 & 0 \end{bmatrix} \tag{12}$$

$$\boldsymbol{g} = \begin{Bmatrix} -\mu(r_c + x)/\rho^{\frac{3}{2}} + \mu/r_c^2 - 2\left(\mu/r_c^3\right)x \\ -\mu y/\rho^{\frac{3}{2}} + \mu y/r_c^3 \\ -\mu z/\rho^{\frac{3}{2}} + \mu z/r_c^3 \end{Bmatrix} \tag{13}$$

If we denote the relative position and velocity tracking error by $\boldsymbol{e}_1$ and $\boldsymbol{e}_2$, respectively, then it is easy to show that the error dynamics can be written as

$$\dot{\boldsymbol{e}}_1 = \boldsymbol{e}_2, \qquad m\dot{\boldsymbol{e}}_2 = m\boldsymbol{A}_1\boldsymbol{x}_1 + m\boldsymbol{A}_2\boldsymbol{x}_2 + m\boldsymbol{g}(\boldsymbol{x}_1) + \boldsymbol{F} - m\ddot{\boldsymbol{x}}_r \tag{14}$$

Now, we augment the system described by Eq. (14) with a passivity-based filter similar to one that was proposed in Refs. 14 and 20. The filter generates the pseudo-velocity estimates and is governed by the following differential equation:

$$\dot{\boldsymbol{z}} = \boldsymbol{A}_m\boldsymbol{z} + \boldsymbol{e}_1 \tag{15}$$

where $\boldsymbol{z} \in \Re^3$ and $\boldsymbol{A}_m$ is any prescribed Hurwitz matrix that satisfies the following Lyapunov equation:

$$\boldsymbol{A}_m^T\boldsymbol{P} + \boldsymbol{P}\boldsymbol{A}_m = -\boldsymbol{Q} \tag{16}$$

where both $\boldsymbol{P}$ and $\boldsymbol{Q}$ are symmetric positive definite matrices.

Theorem 1: For the system described by Eqs. (14) and (15) with no information on the spacecraft mass m, if the following control input $\boldsymbol{F}$ is adopted,

$$\boldsymbol{F} = -\boldsymbol{P}\boldsymbol{e}_1 - \boldsymbol{P}(\boldsymbol{A}_m\boldsymbol{z} + \boldsymbol{e}_1) - \hat{m}\boldsymbol{\Psi} \tag{17}$$

where $\boldsymbol{\Psi} = (\boldsymbol{A}_1\boldsymbol{x}_1 + \boldsymbol{A}_2\dot{\boldsymbol{x}}_r + \boldsymbol{g}(\boldsymbol{x}_1) - \ddot{\boldsymbol{x}}_r)$ with the spacecraft mass estimates $\hat{m}$ being updated by the following adaptation law,

$$\dot{\hat{m}} = \Gamma_1\boldsymbol{e}_2^T\boldsymbol{\Psi} \tag{18}$$

where $\Gamma_1 > 0$ is a gain that controls the rate of mass parameter learning, then we can ensure that $\boldsymbol{e}_1 \to 0$ and $\boldsymbol{e}_2 \to 0$ as $t \to \infty$.

proof: Let $\tilde{m} = m - \hat{m}$ and let us consider the following Lyapunov function:

$$V = \tfrac{1}{2}\boldsymbol{e}_1^T\boldsymbol{P}\boldsymbol{e}_1 + \tfrac{1}{2}m\boldsymbol{e}_2^T\boldsymbol{e}_2 + \tfrac{1}{2}\dot{\boldsymbol{z}}^T\boldsymbol{P}\dot{\boldsymbol{z}} + \tfrac{1}{2}\tilde{m}\Gamma_1^{-1}\tilde{m} \tag{19}$$

It should be noted that V is a radially unbounded positive definite function. The time derivative of V along the system trajectories is given by

$$\dot{V} = \boldsymbol{e}_1^T\boldsymbol{P}\dot{\boldsymbol{e}}_1 + \boldsymbol{e}_2^T m\dot{\boldsymbol{e}}_2 + \tfrac{1}{2}\dot{\boldsymbol{z}}^T\boldsymbol{P}\dot{\boldsymbol{z}} + \tfrac{1}{2}\dot{\boldsymbol{z}}^T\boldsymbol{P}\dot{\boldsymbol{z}} + \tilde{m}\Gamma_1^{-1}\dot{\tilde{m}} \tag{20}$$

Now, substitution of Eqs. (14) and (15) into Eq. (20) leads to the following expression for $\dot{V}$:

$$\dot{V} = \boldsymbol{e}_2^T\Big(\boldsymbol{P}\boldsymbol{e}_1 + \boldsymbol{P}\dot{\boldsymbol{z}} + m\boldsymbol{A}_1\boldsymbol{x}_1 + \underbrace{m\boldsymbol{A}_2\boldsymbol{x}_2}_{mA_2\dot{x}_r + mA_2e_2} + m\boldsymbol{g}(\boldsymbol{x}_1) + \boldsymbol{F} - m\ddot{\boldsymbol{x}}_r\Big)$$

$$+ \tfrac{1}{2}\dot{\boldsymbol{z}}^T\underbrace{\left(\boldsymbol{A}_m^T\boldsymbol{P} + \boldsymbol{P}\boldsymbol{A}_m\right)}_{-Q}\dot{\boldsymbol{z}} + \tilde{m}\Gamma_1^{-1}\dot{\tilde{m}} \tag{21}$$

Rearranging the above,

$$\dot{V} = \boldsymbol{e}_2^T(\boldsymbol{P}\boldsymbol{e}_1 + \boldsymbol{P}(\boldsymbol{A}_m\boldsymbol{z} + \boldsymbol{e}_1) + m\boldsymbol{\Psi} + \boldsymbol{F})$$

$$+ \tfrac{1}{2}\dot{\boldsymbol{z}}^T\underbrace{\left(\boldsymbol{A}_m^T\boldsymbol{P} + \boldsymbol{P}\boldsymbol{A}_m\right)}_{-Q}\dot{\boldsymbol{z}} + \tilde{m}\Gamma_1^{-1}\dot{\tilde{m}} \tag{22}$$

Further, substituting for $\boldsymbol{F}$ from Eq. (17) leads to the following expression:

$$\dot{V} = -\tfrac{1}{2}\dot{\boldsymbol{z}}^T\boldsymbol{Q}\dot{\boldsymbol{z}} + \tilde{m}\left(\boldsymbol{e}_2^T\boldsymbol{\Psi} + \Gamma_1^{-1}\dot{\hat{m}}\right) \tag{23}$$

We can show that choosing the adaptive law from Eq. (18) yields

$$\dot{V} = -\tfrac{1}{2}\dot{\boldsymbol{z}}^T\boldsymbol{Q}\dot{\boldsymbol{z}} \le 0 \tag{24}$$

Because $\dot{V} \le 0$ and $V > 0$, $\dot{V}$ is only negative semidefinite. However, we can easily show that $\boldsymbol{e}_1, \boldsymbol{e}_2, \dot{\boldsymbol{z}} \in \boldsymbol{L}_\infty$. Further, from the integral of Eq. (24), it follows that $\dot{\boldsymbol{z}} \in \boldsymbol{L}_\infty \cap \boldsymbol{L}_2$ and therefore from Barbalat's Lemma[26,27] $\dot{\boldsymbol{z}} \to 0$ as $t \to \infty$. Now, considering higher-order time derivatives of $\dot{\boldsymbol{z}}$ and using uniform continuity arguments similar to those in Refs. 21 and 24, as well as repeated application of Barbalat's lemma, we can show that $\boldsymbol{e}_2 \to 0$. Finally, using LaSalle's invariance principle,[27] we can show that $\boldsymbol{e}_1 \to 0$ as $t \to \infty$.[26,28] Further, from Eq. (15), we can also conclude that $\boldsymbol{z} \to 0$ as $t \to \infty$. □

Remarks:

1) The mass update law in Eq. (18) is used only for analysis. It should be noted that the update law defined in Eq. (18) depends upon the unknown vector $\boldsymbol{e}_2$; therefore for actual implementation of the control law given in Eq. (17), the following equivalent equation should be used, which can be integrated to get the estimated mass parameter:

$$\hat{m}(t) = \hat{m}(0) + \Gamma_1\int_0^t \boldsymbol{\Psi}^T\dot{\boldsymbol{e}}_1\,\mathrm{d}\tau$$

$$= \hat{m}(0) + \Gamma_1\int_{e_1(0)}^{e_1(t)} \boldsymbol{\Psi}^T\,\mathrm{d}\boldsymbol{e}_1 \tag{25}$$

It should be noted that in this expression the independent variable, $\mathrm{d}\boldsymbol{e}_1$, is a vector quantity, so the expression is the sum of three different integrals.

2) Although the preceding analysis does not explicitly address the issue of the mass of the satellite becoming negative during the adaptation, the adaptive algorithm implements a parameter projection[25] that ensures that the adaptation is switched off when the mass violates the lower bound constraint.

Stability Analysis in Presence of Measurement Noise

The control and parameter adaptation law formulation in the previous section are based upon the assumption that true position states of the spacecraft are known, but in any real case, only the sensor measurement derived estimates for spacecraft position are available for feedback purposes. Therefore, instead of using Eq. (17) to compute the control input, the following equation is used:

$$\boldsymbol{F} = -\boldsymbol{P}\tilde{\boldsymbol{e}}_1 - \boldsymbol{P}(\boldsymbol{A}_m\tilde{\boldsymbol{z}} + \tilde{\boldsymbol{e}}_1) - \hat{m}(\boldsymbol{A}_1\tilde{\boldsymbol{x}}_1 + \boldsymbol{A}_2\dot{\boldsymbol{x}}_r + \boldsymbol{g}(\tilde{\boldsymbol{x}}_1) - \ddot{\boldsymbol{x}}_r) \tag{26}$$

where $\tilde{\boldsymbol{x}}_1$ is the sensor-measured spacecraft position and can be modeled as follows:

$$\tilde{\boldsymbol{x}}_1 = \boldsymbol{x}_1 + \boldsymbol{\nu} \tag{27}$$

Here $\boldsymbol{\nu}$ represents the sensor measurement error and represents an aggregation of sensor calibration errors, systematic bias in errors, and some stochastic disturbances present in any real sensor measurement. Similarly, $\tilde{z}_i(s) = [1/(s+\lambda_i)]\tilde{\boldsymbol{x}}_1$ is the filtered output response of the passivity-based filter in Eq. (15) in the presence of sensor noise $\boldsymbol{\nu}$. Assuming a Hurwitz diagonal A_m in Eq. (15), λ_i denotes the ith eigenvalue of A_m. We shall now obtain the trajectory tracking error bounds in presence of bounded sensor noise and show that ultimate boundedness of the error signals can be achieved. Let us reconsider the Lyapunov function defined in the earlier sections:

$$V = \tfrac{1}{2}\boldsymbol{e}_1^T\boldsymbol{P}\boldsymbol{e}_1 + m\tfrac{1}{2}\boldsymbol{e}_2^T\boldsymbol{e}_2 + \tfrac{1}{2}\dot{\boldsymbol{z}}^T\boldsymbol{P}\dot{\boldsymbol{z}} + \tfrac{1}{2}\tilde{m}\Gamma_1^{-1}\tilde{m} \tag{28}$$

Differentiating this and evaluating $\dot{V}$ along the system trajectories leads to the following expression for $\dot{V}$:

$$\dot{V} = \boldsymbol{e}_2^T\Big(\boldsymbol{P}\boldsymbol{e}_1 + \boldsymbol{P}\dot{\boldsymbol{z}} + m\boldsymbol{A}_1\boldsymbol{x}_1 + \underbrace{m\boldsymbol{A}_2\boldsymbol{x}_2}_{mA_2\dot{x}_r + mA_2e_2} + m\boldsymbol{g}(\boldsymbol{x}_1) + \boldsymbol{F} - m\ddot{\boldsymbol{x}}_r\Big)$$

$$+ \tfrac{1}{2}\dot{\boldsymbol{z}}^T\underbrace{\left(\boldsymbol{A}_m^T\boldsymbol{P} + \boldsymbol{P}\boldsymbol{A}_m\right)}_{-Q}\dot{\boldsymbol{z}} + \tilde{m}\Gamma_1^{-1}\dot{\tilde{m}}$$

$$= \boldsymbol{e}_2^T\Big(\boldsymbol{P}\boldsymbol{e}_1 + \boldsymbol{P}\dot{\boldsymbol{z}} + m\boldsymbol{A}_1\boldsymbol{x}_1 + \underbrace{m\boldsymbol{A}_2\boldsymbol{x}_2}_{mA_2\dot{x}_r + mA_2e_2} + m\boldsymbol{g}(\boldsymbol{x}_1) - m\ddot{\boldsymbol{x}}_r\Big)$$

$$- \boldsymbol{e}_2^T\Big(\boldsymbol{P}\tilde{\boldsymbol{e}} + \boldsymbol{P}\tilde{\dot{\boldsymbol{z}}} + \hat{m}\boldsymbol{A}_1\tilde{\boldsymbol{x}} + \underbrace{\hat{m}\boldsymbol{A}_2\boldsymbol{x}_2}_{\hat{m}A_2\dot{x}_r + \hat{m}A_2e_2} + \hat{m}\boldsymbol{g}(\tilde{\boldsymbol{x}}_1) - \hat{m}\ddot{\boldsymbol{x}}_r\Big)$$

$$- \tfrac{1}{2}\dot{\boldsymbol{z}}^T\boldsymbol{Q}\dot{\boldsymbol{z}} + \tilde{m}\Gamma_1^{-1}\dot{\tilde{m}} \tag{29}$$

Using Eq. (18) for $\dot{\hat{m}}$, we get

$$\dot{V} = \boldsymbol{e}_2^T\Big(\boldsymbol{P}\boldsymbol{e}_1 + \boldsymbol{P}\dot{\boldsymbol{z}} + m\boldsymbol{A}_1\boldsymbol{x}_1 + \underbrace{m\boldsymbol{A}_2\boldsymbol{x}_2}_{mA_2\dot{x}_r + mA_2e_2} + m\boldsymbol{g}(\boldsymbol{x}_1) - m\ddot{\boldsymbol{x}}_r\Big)$$

$$- \boldsymbol{e}_2^T\Big(\boldsymbol{P}\tilde{\boldsymbol{e}} + \boldsymbol{P}\tilde{\dot{\boldsymbol{z}}} + \hat{m}\boldsymbol{A}_1\tilde{\boldsymbol{x}} + \underbrace{\hat{m}\boldsymbol{A}_2\boldsymbol{x}_2}_{\hat{m}A_2\dot{x}_r + \hat{m}A_2e_2} + \hat{m}\boldsymbol{g}(\tilde{\boldsymbol{x}}_1) - \hat{m}\ddot{\boldsymbol{x}}_r\Big)$$

$$- \tfrac{1}{2}\dot{\boldsymbol{z}}^T\boldsymbol{Q}\dot{\boldsymbol{z}} - \boldsymbol{e}_2^T\tilde{m}\Big(\boldsymbol{A}_1\tilde{\boldsymbol{x}}_1 + \underbrace{\boldsymbol{A}_2\boldsymbol{x}_2}_{A_2\dot{x}_r + A_2e_2} + \boldsymbol{g}(\tilde{\boldsymbol{x}}_1) - \ddot{\boldsymbol{x}}_r\Big) \tag{30}$$

Note: The inclusion of $\boldsymbol{A}_2\boldsymbol{e}_2$ into the terms above does not change anything since the matrix $\boldsymbol{A}_2$ is skew-symmetric. Rearranging the terms above, the time derivative of the Lyapunov function reduces to

$$\dot{V} = \boldsymbol{e}_2^T[\boldsymbol{P}(\boldsymbol{e}_1 - \tilde{\boldsymbol{e}}_1) + \boldsymbol{P}(\dot{\boldsymbol{z}} - \tilde{\dot{\boldsymbol{z}}}) + m\boldsymbol{A}_1(\boldsymbol{x}_1 - \tilde{\boldsymbol{x}}_1)$$

$$+ m(\boldsymbol{g}(\boldsymbol{x}_1) - \boldsymbol{g}(\tilde{\boldsymbol{x}}_1))] - \tfrac{1}{2}\dot{\boldsymbol{z}}^T\boldsymbol{Q}\dot{\boldsymbol{z}} \tag{31}$$

We now assume that the sensor noise $\boldsymbol{\nu}$ is bounded symmetrically by $\boldsymbol{\nu}_u$; that is, $-\boldsymbol{\nu}_u \le \boldsymbol{\nu} \le \boldsymbol{\nu}_u$, so that $[\boldsymbol{x}_1 - \boldsymbol{\nu}_u, \boldsymbol{x}_1 + \boldsymbol{\nu}_u]$ is a compact interval around the operating point $\boldsymbol{x}_1$. Furthermore, assuming that $\boldsymbol{g}(.) \in \mathcal{C}^1$, that is, the derivative of $\boldsymbol{g}(.)$ exists and satisfies $\|\boldsymbol{g}'(.)\| \le M_g$, we can use the mean value theorem[29] to bound the nonlinear vector $\boldsymbol{g}(.)$ as follows:

$$\|\boldsymbol{g}(\boldsymbol{x}_1) - \boldsymbol{g}(\tilde{\boldsymbol{x}}_1)\| \le M_g\|\boldsymbol{x}_1 - \tilde{\boldsymbol{x}}_1\| \tag{32}$$

Because $\tilde{z}(s) = [1/(s+\lambda_i)]\tilde{\boldsymbol{x}}_1(s)$ and $\boldsymbol{z}(s) = [1/(s+\lambda_i)]\boldsymbol{x}_1(s)$, we see that $\bar{z}(s) \triangleq \tilde{z}(s) - z(s) = [1/(s+\lambda_i)](\tilde{\boldsymbol{x}}_1(s) - \boldsymbol{x}_1(s)) = [1/(s+\lambda_i)]\boldsymbol{\nu}(s)$. Because the sensor noise is assumed to be bounded,

we conclude that

$$\|z-\tilde{z}\| \le M_z \|x_1 - \tilde{x}_1\| \tag{33}$$

Now, from Eqs. (31), (32), and (33), we can rewrite $\dot{V}$ as

$$|\dot{V}| \le \|e_2\|[|\lambda_{\max}(P)|\{\|\nu_u\| + M_z\|\nu_u\|\} + M_u\{\|A_1\| + M_g\}\|\nu_u\|] - \tfrac{1}{2}|\lambda_{\min}(Q)|\|\dot{z}\|^2$$

$$|\dot{V}| \le \|e_2\| \underbrace{[|\lambda_{\max}(P)|(1+M_z) + M_u(\|A_1\| + M_g)]}_{\Phi} \|\nu_u\| - \tfrac{1}{2}|\lambda_{\min}(Q)|\|\dot{z}\|^2$$

Remarks:

1) M_u is the upper bound on the spacecraft mass. Even though the spacecraft mass is not known, we assume an upper bound is available a priori.

2) From Eq. (11), we see that A_1 depends on the reference orbit parameters. We can easily construct an upper bound on this matrix based on the reference orbit characteristics. Let A_{1F} denote the upper bound on A_1.

Thus, this equation can be rewritten as

$$|\dot{V}| \le -\tfrac{1}{2}|\lambda_{\min}(Q)|\|\dot{z}\|^2 + \|e_2\|\Phi\|\nu_u\| \tag{34}$$

where $\Phi = |\lambda_{\max}(P)|(1+M_z) + M_u(A_{1F} + M_g)$.

Note:

1) When $\nu_u = 0$, that is, the position measurements are perfect, we recover the earlier situation (no noise) and the ideal global asymptotic stability guarantees.

2) For a given level of measurement noise, we can only conclude bounded stability, so long as the translational velocity tracking error satisfies the following bound:

$$\|e_2\| \le [|\lambda_{\min}(Q)|/2\Phi][\|\dot{z}\|^2/\|\nu_u\|] \tag{35}$$

Further, making use of the filter equation, we have

$$\|e_2\| \le [|\lambda_{\min}(Q)|/2\Phi][\|A_m z + e_1\|^2/\|\nu_u\|] \tag{36}$$

It is evident that with perfect or very good sensors, the tolerable velocity errors are also higher. This inequality reiterates the importance of accurate measurements and the bound can theoretically accommodate infinite velocity errors if $\nu_u = 0$.

It should be noted that initially, one can always maintain the bound in Eq. (36) by a judicious choice of A_m and Q matrices. However, with the passage of time the right-hand side of Eq. (36) decreases as e_1 decreases but one can maintain this bound if e_2 decreases at a faster rate than e_1, which is usually the case. However, if the bound in Eq. (36) is violated the mass estimates $\hat{m}$ may drift to infinity with time. To accommodate these one can set an upper bound M on $\hat{m}$. Thus the modified adaptation law is

$$\dot{\hat{m}} = \begin{cases} \Gamma_1 e_2^T \Psi, & \text{if } \|e_2\| \le \dfrac{|\lambda_{\min}(Q)|}{2\Phi}\dfrac{\|A_m z + e_1\|^2}{\|\nu_u\|} \quad \text{and} \quad \hat{m} \le M \\ 0, & \text{otherwise} \end{cases} \tag{37}$$

According to this modified update law for $\hat{m}$, if $\|e_2\| \le [|\lambda_{\min}(Q)|/2\Phi](\|A_m z + e_1\|^2/\|\nu_u\|)$, then $\dot{V}$ is always negative semidefinite and stability arguments are the same as in the last section. However, in the case where the bound in Eq. (36) is violated, the mass estimates $\hat{m}$ and e_1 may increase as $\dot{V} > 0$ but both the quantities are still bounded due to the adaptation law in Eq. (37). If the bound on $\|e_2\|$ is too large, this means that we need position measurement sensors with better noise properties.

3) It should be also mentioned that the analysis in this section can be used to choose position measurement sensors to satisfy the following bound:

$$\|\nu_u\| \le [|\lambda_{\min}(Q)|/2\Phi]\left[\|\dot{z}\|^2 \big/ \|e_2\|\right] \tag{38}$$

From the filter equation we have, $e_2 = \ddot{z} - A_m\dot{z}$. Without loss of generality, assuming that $A_m = -\lambda I_{3\times 3}$, $\lambda > 0$, we have $e_2 = (\mathrm{d}/\mathrm{d}t)(\dot{z} + \lambda z)$. Thus, the inequality in Eq. (38) can be rewritten as

$$\|\nu_u\| \le \frac{|\lambda_{\min}(Q)|}{2\Phi}\frac{\|\dot{z}\|^2}{\|(\mathrm{d}/\mathrm{d}t)(\dot{z} + \lambda z)\|} \tag{39}$$

Note the above inequality allow us to compute the bound on measurement error given the desired performance of the controller.

Finally, it should be noted that the analysis presented in this section only assumes that sensor noise is bounded in magnitude, that is, signal-to-noise ratio is bounded. Therefore, the analysis presented in this section can be used to evaluate the controller performance in the presence of large class of measurement errors (systematic or stochastic). Generally, sensor errors are modeled by a Gaussian white noise process and in that case the upper bound ν can be easily related, at least approximately, to a suitably large multiple of the standard deviation of the white noise. In summary, the analysis presented in this section allows us to tie the stability analysis of the controller performance to sensor measurement accuracy.

Adaptive Control Formulation for Rotation Motion Maneuver

In this section, we present the adaptive control law formulation for attitude control. By utilizing thrusters for translational control and reaction wheels for attitude control, we can uncouple the translational and rotational control to a high degree of approximation. We seek a control law for the system described by Eqs. (6) and (7) to track a given trajectory specified by σ_r. This control law formulation is similar to the one presented in Refs. 24 and 28. The novel feature of the control law presented in this paper is that it not only addresses the uncertainties in the modeling of the momentum wheels dynamics due to unknown wheel inertia or misalignment with the spacecraft body axes but it also addresses the uncertainties present in the state vector measurements/estimates. The control law and stability analysis for the zero measurement noise is presented first and the stability proofs are rederived in the next section for the case when the measurement noise is present.

To construct the output feedback adaptive controller, we augment the error dynamics with a low-pass filter analogous to the one presented in the previous section:

$$\dot{z} = A_m z + e \tag{40}$$

$$A_m^T P + P A_m = -Q \tag{41}$$

where A_m is Hurwitz whereas P and Q are positive definite symmetric matrices.

Theorem 2: For the system described by Eqs. (6), (7), and (40) with no a priori information about the spacecraft mass inertia and reaction wheel inertia matrices I and A, the following control input $\dot{\Omega}$,

$$\dot{\Omega} = \hat{A}^{-1}\left[\hat{d} + \tfrac{1}{4}J^T(e)P\dot{z} + \tfrac{1}{4}J^T(e)Pe - \hat{I}C(e)\dot{\omega}_r - [\tilde{\eta}](\hat{A}\Omega + \hat{I}\eta)\right] \tag{42}$$

with the estimates $\hat{I}(t)$ and $\hat{A}(t)$ updated according to the following adaption law,

$$\dot{\hat{\theta}} = \Gamma_1 W_d^T \delta\omega \tag{43}$$

where $\theta \in \Re^{15}$, is a parameter vector consisting of uncertain spacecraft inertia, wheel inertia, and disturbance terms:

$$\boldsymbol{\theta} = \begin{Bmatrix} I_{11} & I_{12} & I_{13} & I_{22} & I_{23} & I_{33} & A_{11} & A_{12} & A_{13} & A_{22} & A_{23} & A_{33} & d_1 & d_2 & d_3 \end{Bmatrix}^T \tag{44}$$

$\boldsymbol{W}_d \in \Re^{3\times 15}$, the regressor matrix,[24] is defined as

$$\boldsymbol{W}_{d1} = \begin{bmatrix} cw_1 & cw_2 & cw_3 & 0 & 0 & 0 \\ 0 & cw_1 & 0 & cw_2 & cw_3 & 0 \\ 0 & 0 & cw_1 & 0 & cw_2 & cw_3 \end{bmatrix}, \qquad \boldsymbol{cw} = \boldsymbol{C}(\boldsymbol{e})\dot{\omega}_r \tag{45}$$

$$\boldsymbol{W}_{d2} = \begin{bmatrix} 0 & -\Omega_1\eta_3 & \Omega_1\eta_2 & -\Omega_2\eta_3 & -\Omega_3\eta_3 + \Omega_2\eta_2 & \Omega_3\eta_2 \\ \Omega_1\eta_3 & \Omega_2\eta_3 & \Omega_3\eta_3 - \Omega_1\eta_1 & 0 & -\Omega_2\eta_1 & -\Omega_3\eta_1 \\ \Omega_1\eta_2 & -\Omega_2\eta_2 + \Omega_1\eta_1 & -\Omega_3\eta_2 & \Omega_2\eta_1 & \Omega_3\eta_1 & 0 \end{bmatrix} \tag{46}$$

$$\boldsymbol{W}_{d3} = \begin{bmatrix} 0 & -\eta_1\eta_3 & \eta_1\eta_2 & -\eta_2\eta_3 & -\eta_3\eta_3 + \eta_2\eta_2 & \eta_3\eta_2 \\ \eta_1\eta_3 & \eta_2\eta_3 & \eta_3\eta_3 - \eta_1\eta_1 & 0 & -\eta_2\eta_1 & -\eta_3\eta_1 \\ \eta_1\eta_2 & -\eta_2\eta_2 + \eta_1\eta_1 & -\eta_3\eta_2 & \eta_2\eta_1 & \eta_3\eta_1 & 0 \end{bmatrix} \tag{47}$$

$$\boldsymbol{W}_{d4} = \begin{bmatrix} u_1 & u_2 & u_3 & 0 & 0 & 0 \\ 0 & u_1 & 0 & u_2 & u_3 & 0 \\ 0 & 0 & u_1 & 0 & u_2 & u_3 \end{bmatrix}, \qquad \boldsymbol{u} = \dot{\boldsymbol{\Omega}} \tag{48}$$

$$\boldsymbol{W}_d = \begin{bmatrix} -\boldsymbol{W}_{d1} - \boldsymbol{W}_{d3} & -\boldsymbol{W}_{d2} - \boldsymbol{W}_{d2} & \boldsymbol{I}_{3\times 3} \end{bmatrix} \tag{49}$$

and $\boldsymbol{\Gamma}_1 \in \Re^{15\times 15}$ as any positive definite symmetric matrix, we can ensure that $\boldsymbol{e} \to 0$ and $\delta\omega \to 0$ as $t \to \infty$.

Psroof: Let us consider the following candidate Lyapunov function:

$$V = \tfrac{1}{2}\boldsymbol{e}^T\boldsymbol{P}\boldsymbol{e} + \tfrac{1}{2}\boldsymbol{\delta\omega}^T\boldsymbol{I}\boldsymbol{\delta\omega} + \tfrac{1}{2}\dot{\boldsymbol{z}}^T\boldsymbol{P}\dot{\boldsymbol{z}} + \tfrac{1}{2}\tilde{\boldsymbol{\theta}}^T\Gamma_1^{-1}\tilde{\boldsymbol{\theta}} \tag{50}$$

where V is radially unbounded and positive. The time derivative of V along the system trajectories is given by

$$\dot{V} = \boldsymbol{e}^T\boldsymbol{P}\dot{\boldsymbol{e}} + \boldsymbol{\delta\omega}^T\boldsymbol{I}\boldsymbol{\delta\dot{\omega}} + \tfrac{1}{2}\ddot{\boldsymbol{z}}^T\boldsymbol{P}\dot{\boldsymbol{z}} + \tfrac{1}{2}\dot{\boldsymbol{z}}^T\boldsymbol{P}\ddot{\boldsymbol{z}} + \tilde{\boldsymbol{\theta}}^T\Gamma_1^{-1}\dot{\tilde{\boldsymbol{\theta}}} \tag{51}$$

Now, substitution of Eqs. (6) and (7) into Eq. (51) leads to the following expression for $\dot{V}$:

$$\dot{V} = \boldsymbol{\delta\omega}^T\left(\tfrac{1}{4}\boldsymbol{J}^T(\boldsymbol{e})\boldsymbol{P}\boldsymbol{e} + \tfrac{1}{4}\boldsymbol{J}^T(\boldsymbol{e})\boldsymbol{P}\dot{\boldsymbol{z}} - [\tilde{\omega}]\boldsymbol{I}\boldsymbol{\omega} - \boldsymbol{A}\dot{\boldsymbol{\Omega}} - [\tilde{\omega}]\boldsymbol{A}\boldsymbol{\Omega} + \boldsymbol{d}\right.$$
$$\left. - \boldsymbol{I}[\boldsymbol{C}(\boldsymbol{e})\dot{\omega}_r - [\tilde{\omega}]\boldsymbol{\eta}]\right) + \tfrac{1}{2}\dot{\boldsymbol{z}}^T\underbrace{\left(\boldsymbol{A}_m^T\boldsymbol{P} + \boldsymbol{P}\boldsymbol{A}_m\right)}_{-Q}\dot{\boldsymbol{z}} + \tilde{\boldsymbol{\theta}}^T\Gamma_1^{-1}\dot{\tilde{\boldsymbol{\theta}}} \tag{52}$$

Now, substituting of Eq. (42) into this equation and after some algebraic manipulations, we can show that

$$\dot{V} = \delta\boldsymbol{\omega}^T[-[\tilde{\eta}]\tilde{\boldsymbol{A}}\boldsymbol{\Omega} + [\tilde{\eta}]\tilde{\boldsymbol{I}}\boldsymbol{\eta} + \tilde{\boldsymbol{d}} - \tilde{\boldsymbol{I}}\boldsymbol{C}(\boldsymbol{e})\dot{\omega}_r - \tilde{\boldsymbol{A}}\boldsymbol{u}]$$
$$+ \delta\boldsymbol{\omega}^T[-[\tilde{\omega}]\boldsymbol{I}\boldsymbol{\omega} + [\boldsymbol{A}\tilde{\boldsymbol{\Omega}}]\delta\boldsymbol{\omega} + \boldsymbol{I}[\tilde{\omega}]\boldsymbol{\eta} + [\tilde{\eta}]\boldsymbol{I}\boldsymbol{\eta}]$$
$$- \tfrac{1}{2}\dot{\boldsymbol{z}}^T\boldsymbol{Q}\dot{\boldsymbol{z}} + \tilde{\boldsymbol{\theta}}^T\Gamma_1^{-1}\dot{\tilde{\boldsymbol{\theta}}} \tag{53}$$

Further, using Eqs. (45–49) and adopting the adaptation law for $\dot{\hat{\theta}}$ given by Eq. (43), we get the following expression for $\dot{V}$:

$$\dot{V} = -\tfrac{1}{2}\dot{\boldsymbol{z}}^T\boldsymbol{Q}\dot{\boldsymbol{z}} + \delta\boldsymbol{\omega}^T(-[\tilde{\omega}]\boldsymbol{I}\boldsymbol{\omega} + \boldsymbol{I}[\tilde{\omega}]\boldsymbol{\eta} + [\tilde{\eta}]\boldsymbol{I}\boldsymbol{\eta}) \tag{54}$$

Using Eq. (5), it can be proved that the second term on the right-hand side is identically equal to zero. Therefore, the equation for $\dot{V}$ reduces to the equation

$$\dot{V} = -\tfrac{1}{2}\dot{\boldsymbol{z}}^T\boldsymbol{Q}\dot{\boldsymbol{z}} \le 0 \tag{55}$$

Because $\dot{V} \le 0$ and $V > 0$, we can easily show that $\boldsymbol{e}, \boldsymbol{\delta\omega}, \dot{\boldsymbol{z}}, \tilde{\boldsymbol{\theta}} \in \boldsymbol{L}_\infty$. Further, from the integral of Eq. (55), it follows that $\dot{\boldsymbol{z}} \in \boldsymbol{L}_2 \cap \boldsymbol{L}_\infty$ and therefore from Barbalat's lemma $\dot{\boldsymbol{z}} \to 0$ as $t \to \infty$. Now using the uniform continuity arguments similar to that in Refs. 24 and 21, we conclude that $\dot{\boldsymbol{e}} \to 0$ and $\boldsymbol{\delta\omega} \to 0$ based on Eqs. (6). Further, by repeated application of the uniform continuity argument and Barbalat's lemma to the higher derivatives of $\boldsymbol{z}$, we can show that $\boldsymbol{\dot{\delta}\omega} \to 0$ and then by straightforward application of LaSalle's invariance principle[26] we can show that $\boldsymbol{e} \to 0$ and $\boldsymbol{\delta\omega} \to 0$ as $t \to \infty$.[21,24,28] □

Stability Analysis in the Presence of Measurement Noise

The control and parameter adaptation law formulation in the last section were based upon the assumption that the true attitude states of the spacecraft were known, but in the real case only the sensor measurements for the spacecraft attitude are available. Therefore, instead of using Eq. (42) to compute the actuator response, the following equation is used:

$$\dot{\boldsymbol{\Omega}} = \hat{\boldsymbol{A}}^{-1}\left[\hat{\boldsymbol{d}} + \tfrac{1}{4}\boldsymbol{J}^T(\tilde{\boldsymbol{e}})\boldsymbol{P}\dot{\boldsymbol{z}} + \tfrac{1}{4}\boldsymbol{J}^T(\tilde{\boldsymbol{e}})\boldsymbol{P}\tilde{\boldsymbol{e}} - \hat{\boldsymbol{I}}\boldsymbol{C}(\tilde{\boldsymbol{e}})\dot{\omega}_r - [\tilde{\eta}](\hat{\boldsymbol{A}}\tilde{\boldsymbol{\Omega}} + \hat{\boldsymbol{I}}\boldsymbol{\eta})\right] \tag{56}$$

where $\tilde{\boldsymbol{e}}$ denotes the spacecraft attitude error obtained from the attitude sensor and $\tilde{\boldsymbol{\Omega}}$ represents the measured wheel speed, which are modeled as the following measurement quantities:

$$\tilde{\boldsymbol{e}} = \boldsymbol{e} + \boldsymbol{\nu}_e \tag{57}$$

$$\tilde{\boldsymbol{\Omega}} = \boldsymbol{\Omega} + \boldsymbol{\nu}_w \tag{58}$$

where $\boldsymbol{\nu}_e$ and $\boldsymbol{\nu}_w$ represent attitude sensor noise and rotation wheel sensor noise vectors, respectively. To obtain the error bounds in the presence of sensor noise, let us consider the candidate Lyapunov function proposed earlier:

$$V = \tfrac{1}{2}\boldsymbol{e}^T\boldsymbol{P}\boldsymbol{e} + \tfrac{1}{2}\boldsymbol{\delta\omega}^T\boldsymbol{I}\boldsymbol{\delta\omega} + \tfrac{1}{2}\dot{\boldsymbol{z}}^T\boldsymbol{P}\dot{\boldsymbol{z}} + \tfrac{1}{2}\tilde{\boldsymbol{\theta}}^T\Gamma_1^{-1}\tilde{\boldsymbol{\theta}} \tag{59}$$

The time derivative of V along the system trajectories is given by

$$\dot{V} = \boldsymbol{e}^T\boldsymbol{P}\dot{\boldsymbol{e}} + \boldsymbol{\delta\omega}^T\boldsymbol{I}\boldsymbol{\delta\dot{\omega}} + \tfrac{1}{2}\ddot{\boldsymbol{z}}^T\boldsymbol{P}\dot{\boldsymbol{z}} + \tfrac{1}{2}\dot{\boldsymbol{z}}^T\boldsymbol{P}\ddot{\boldsymbol{z}} + \tilde{\boldsymbol{\theta}}^T\Gamma_1^{-1}\dot{\tilde{\boldsymbol{\theta}}} \tag{60}$$

Now, substitution of Eqs. (6) and (7) into Eq. (60) leads to the following expression for $\dot{V}$:

$$\dot{V} = \boldsymbol{\delta\omega}^T\left(\tfrac{1}{4}\boldsymbol{J}^T(\boldsymbol{e})\boldsymbol{P}\boldsymbol{e} + \tfrac{1}{4}\boldsymbol{J}^T(\boldsymbol{e})\boldsymbol{P}\dot{\boldsymbol{z}} - [\tilde{\omega}]\boldsymbol{I}\boldsymbol{\omega} - \boldsymbol{A}\dot{\boldsymbol{\Omega}} - [\tilde{\omega}]\boldsymbol{A}\boldsymbol{\Omega} + \boldsymbol{d}\right.$$
$$\left. - \boldsymbol{I}[\boldsymbol{C}(\boldsymbol{e})\dot{\omega}_r - [\tilde{\omega}]\boldsymbol{\eta}]\right) + \tfrac{1}{2}\dot{\boldsymbol{z}}^T\underbrace{\left(\boldsymbol{A}_m^T\boldsymbol{P} + \boldsymbol{P}\boldsymbol{A}_m\right)}_{-Q}\dot{\boldsymbol{z}} + \tilde{\boldsymbol{\theta}}^T\Gamma_1^{-1}\tilde{\boldsymbol{\theta}} \tag{61}$$

Further, substituting for $\dot{\boldsymbol{\Omega}}$ from Eq. (56) in the above equation and some algebraic manipulations lead to the following expression:

$$\dot{V} = \delta\boldsymbol{\omega}^T[-[\tilde{\boldsymbol{\eta}}]\tilde{\boldsymbol{A}}\boldsymbol{\Omega} + [\tilde{\boldsymbol{\eta}}]\tilde{\boldsymbol{I}}\boldsymbol{\eta} + \tilde{\boldsymbol{d}} - \tilde{\boldsymbol{I}}\boldsymbol{C}(\boldsymbol{e})\dot{\boldsymbol{\omega}}_r - \tilde{\boldsymbol{A}}\boldsymbol{u}] + \delta\boldsymbol{\omega}^T[-[\tilde{\boldsymbol{\omega}}]\boldsymbol{I}\boldsymbol{\omega} + [\boldsymbol{A}\tilde{\boldsymbol{\Omega}}]\delta\boldsymbol{\omega} + \boldsymbol{I}[\tilde{\boldsymbol{\omega}}]\boldsymbol{\eta} + [\tilde{\boldsymbol{\eta}}]\boldsymbol{I}\boldsymbol{\eta}] + \delta\boldsymbol{\omega}^T\big(\hat{\boldsymbol{I}}[\boldsymbol{C}(\tilde{\boldsymbol{e}}) - \boldsymbol{C}(\boldsymbol{e})]\dot{\boldsymbol{\omega}}_r + [\tilde{\boldsymbol{\eta}}]\hat{\boldsymbol{A}}[\tilde{\boldsymbol{\Omega}} - \boldsymbol{\Omega}] + \tfrac{1}{4}\boldsymbol{J}(\boldsymbol{e})\boldsymbol{P}(\boldsymbol{e} + \dot{\boldsymbol{z}}) - \tfrac{1}{4}\boldsymbol{J}(\tilde{\boldsymbol{e}})\boldsymbol{P}(\tilde{\boldsymbol{e}} + \dot{\tilde{\boldsymbol{z}}})\big) - \tfrac{1}{2}\dot{\boldsymbol{z}}^T\boldsymbol{Q}\dot{\boldsymbol{z}} + \tilde{\boldsymbol{\theta}}^T\Gamma_1^{-1}\dot{\tilde{\boldsymbol{\theta}}} \tag{62}$$

Now, adopting the adaptation law for $\dot{\tilde{\boldsymbol{\theta}}}$ from Eq. (43) and using the fact that the second term in the above equation is identically zero, we get

$$\dot{V} = \delta\boldsymbol{\omega}^T\big(\hat{\boldsymbol{I}}[\boldsymbol{C}(\tilde{\boldsymbol{e}}) - \boldsymbol{C}(\boldsymbol{e})]\dot{\boldsymbol{\omega}}_r + [\tilde{\boldsymbol{\eta}}]\hat{\boldsymbol{A}}[\tilde{\boldsymbol{\Omega}} - \boldsymbol{\Omega}] + \tfrac{1}{4}[\boldsymbol{J}(\boldsymbol{e}) - \boldsymbol{J}(\tilde{\boldsymbol{e}})] \times \boldsymbol{P}(\boldsymbol{e} + \dot{\boldsymbol{z}}) - \tfrac{1}{4}\boldsymbol{J}(\tilde{\boldsymbol{e}})\boldsymbol{P}(\tilde{\boldsymbol{e}} - \boldsymbol{e}) - \tfrac{1}{4}\boldsymbol{J}(\tilde{\boldsymbol{e}})\boldsymbol{P}(\dot{\tilde{\boldsymbol{z}}} - \dot{\boldsymbol{z}})\big) - \tfrac{1}{2}\dot{\boldsymbol{z}}^T\boldsymbol{Q}\dot{\boldsymbol{z}} \tag{63}$$

where the sensor noise vectors $\boldsymbol{\nu}_e$ and $\boldsymbol{\nu}_w$ are bounded by $\boldsymbol{\nu}_{e_u}$ and $\boldsymbol{\nu}_{w_u}$, respectively, so that $[\boldsymbol{e} - \boldsymbol{\nu}_{e_u}, \boldsymbol{e} + \boldsymbol{\nu}_{e_u}]$ and $[\boldsymbol{\Omega} - \boldsymbol{\nu}_{w_u}, \boldsymbol{\Omega} + \boldsymbol{\nu}_{w_u}]$ are compact intervals. We use the mean value theorem to construct the following bounds:

$$\|\boldsymbol{J}(\tilde{\boldsymbol{e}}) - \boldsymbol{J}(\boldsymbol{e})\| \le M_J\|\tilde{\boldsymbol{e}} - \boldsymbol{e}\| \tag{64}$$

$$\|\boldsymbol{C}(\tilde{\boldsymbol{e}}) - \boldsymbol{C}(\boldsymbol{e})\| \le M_C\|\tilde{\boldsymbol{e}} - \boldsymbol{e}\| \tag{65}$$

$$\|\boldsymbol{z}(\tilde{\boldsymbol{e}}) - \boldsymbol{z}(\boldsymbol{e})\| \le M_z\|\tilde{\boldsymbol{e}} - \boldsymbol{e}\| \tag{66}$$

Remarks:

1) $\boldsymbol{J}(.)$, $\boldsymbol{C}(.)$, and $\boldsymbol{z}(.)$ are $\mathcal{C}^1$ functions; that is, their first derivatives exist and are bounded by M_J, M_C, and M_z respectively.

2) For the range of nonsingular attitude motion, that is, for the principal rotation angle up to 2π, the bound $\boldsymbol{M}_J$ can always be constructed.

3) Because $\boldsymbol{C}(.)$ is the rotation matrix, the upper bound is easily constructed.

Now, using Eqs. (64–66), we can rewrite bound $|\dot{V}|$ as

$$|\dot{V}| \le \big(\lambda_{\max}(\hat{\boldsymbol{I}})M_C\|\dot{\boldsymbol{\omega}}_r\| - \tfrac{1}{4}\lambda_{\min}(\boldsymbol{P})M_J\|(\boldsymbol{e} + \dot{\boldsymbol{z}})\| - \tfrac{1}{4}\lambda_{\min}(\boldsymbol{P})\|\boldsymbol{J}(\tilde{\boldsymbol{e}})\|(1 + M_z)\big)\|\tilde{\boldsymbol{e}} - \boldsymbol{e}\|\|\delta\boldsymbol{\omega}\| + \|[\tilde{\boldsymbol{\eta}}]\hat{\boldsymbol{A}}\|\|\tilde{\boldsymbol{\Omega}} - \boldsymbol{\Omega}\|\|\delta\boldsymbol{\omega}\| - \tfrac{1}{2}\lambda_{\min}(\boldsymbol{Q})\|\dot{\boldsymbol{z}}\|^2 \tag{67}$$

Now using the fact that $\|\tilde{\boldsymbol{e}} - \boldsymbol{e}\| = \|\boldsymbol{\nu}_e\| \le \|\boldsymbol{\nu}_{e_u}\|$, we can rewrite this equation as

$$|\dot{V}| \le \underbrace{\big(\lambda_{\max}(\hat{\boldsymbol{I}})M_C\|\dot{\boldsymbol{\omega}}_r\| - \tfrac{1}{4}\lambda_{\min}(\boldsymbol{P})M_J\|(\boldsymbol{e} + \dot{\boldsymbol{z}})\| - \tfrac{1}{4}\lambda_{\min}(\boldsymbol{P})\|\boldsymbol{J}(\tilde{\boldsymbol{e}})\|(1 + M_z)\big)}_{\Phi_e}\|\boldsymbol{\nu}_{e_u}\|\|\delta\boldsymbol{\omega}\| + \underbrace{\|\text{skew}\{\boldsymbol{C}(\boldsymbol{e})\omega_r\}\hat{\boldsymbol{A}}\|}_{\Phi_w}\|\boldsymbol{\nu}_{w_u}\|\|\delta\boldsymbol{\omega}\| - \tfrac{1}{2}\lambda_{\min}(\boldsymbol{Q})\|\dot{\boldsymbol{z}}\|^2$$

$$\le -\tfrac{1}{2}\lambda_{\min}(\boldsymbol{Q})\|\dot{\boldsymbol{z}}\|^2 + \{\boldsymbol{\Phi}_e\|\boldsymbol{\nu}_{e_u}\| + \boldsymbol{\Phi}_w\|\boldsymbol{\nu}_{w_u}\|\}\|\delta\boldsymbol{\omega}\| \tag{68}$$

Note:

1) When $\boldsymbol{\nu}_{e_u} = 0$ and $\boldsymbol{\nu}_{w_u} = 0$, that is, the measurements are perfect, we recover the ideal global asymptotic stability guarantees.

2) For a given level of the measurement noise, we can only conclude bounded stability, so long as the angular velocity tracking error satisfies satisfies the following bound:

$$\|\delta\boldsymbol{\omega}\| \le \Big(\frac{|\lambda_{\min}(\boldsymbol{Q})|}{2\Phi}\Big)\Big(\frac{\|\dot{\boldsymbol{z}}\|^2}{\boldsymbol{\Phi}_e\|\boldsymbol{\nu}_{e_u}\| + \boldsymbol{\Phi}_w\|\boldsymbol{\nu}_{w_u}\|}\Big) = \delta\omega_u \tag{69}$$

It is evident that with perfect or very good sensors, the tolerable velocity errors are also higher. The above inequality reiterates the importance of accurate measurements and the bound can theoretically accommodate infinite velocity errors if $\boldsymbol{\nu}_{e_u} = 0$ and $\boldsymbol{\nu}_{w_u} = 0$.

It should be noted that the bound in Eq. (69) can be maintained by judicious choice of controller tuning parameters, for example, $\boldsymbol{A}_m$ and $\boldsymbol{Q}$ matrices. However, if the bound in Eq. (69) is violated then uncertain parameter estimates, $\hat{\boldsymbol{\theta}}$ may drift to infinity with time. To take care of this rare but possible case one can set an upper bound Θ on $\|\hat{\boldsymbol{\theta}}\|$. Thus the modified adaptation law is

$$\dot{\hat{\boldsymbol{\theta}}} = \begin{cases} \Gamma_1\boldsymbol{W}_d^T\boldsymbol{J}^{-1}(\boldsymbol{e})\dot{\boldsymbol{e}} & \text{if} \quad \|\delta\boldsymbol{\omega}\| \le \delta\omega_u \quad \text{and} \quad \|\hat{\boldsymbol{\theta}}\| \le \Theta \\ 0 & \text{otherwise} \end{cases} \tag{70}$$

According to this modified update law for $\hat{\boldsymbol{\theta}}$, if $\|\delta\boldsymbol{\omega}\| \le \delta\omega_u$, then $\dot{V}$ is always negative semidefinite and the stability arguments are same as in the last section. The uncertain system parameter estimates, $\hat{\boldsymbol{\theta}}$ and tracking error, $\boldsymbol{e}_1$ may increase whenever the bound in Eq. (69) is violated. However, both the quantities are still bounded due to adaptation law in Eq. (70) and it means that we need position measurement sensor with better noise properties.

3) Finally, the analysis presented in this section can be used to choose measurement sensors to satisfy the following bound:

$$\boldsymbol{\Phi}_e\|\boldsymbol{\nu}_{e_u}\| + \boldsymbol{\Phi}_w\|\boldsymbol{\nu}_{w_u}\| \le [|\lambda_{\min}(\boldsymbol{Q})|/2\Phi][\|\dot{\boldsymbol{z}}\|^2/\|\delta\boldsymbol{\omega}\|] \tag{71}$$

Note that this inequality allow us to compute the bound on measurement error given the desired performance of the controller.

Once again, it should be noted that the update law defined in Eq. (43) depends upon the unknown vector $\boldsymbol{\delta\omega}$; therefore, for actual implementation of the control law given in Eq. (42), the following equivalent equation should be used, which can be integrated to get the estimated inertia parameters:

$$\hat{\boldsymbol{\theta}}(t) = \hat{\boldsymbol{\theta}}(t)(0) + \Gamma_1\int_0^t \boldsymbol{W}_d^T\boldsymbol{J}^{-1}(\boldsymbol{e})\dot{\boldsymbol{e}}\,\mathrm{d}t = \hat{\boldsymbol{\theta}}(t)(0) + \Gamma_1\int_0^{\boldsymbol{e}} \boldsymbol{W}_d^T\boldsymbol{J}^{-1}(\boldsymbol{e})\,\mathrm{d}\boldsymbol{e} \tag{72}$$

The adaptation laws presented in this paper do not guarantee the convergence of the unknown mass and inertia parameters to their true values but ensure that the parameter estimation errors are bounded. Furthermore, the adaptation laws do not guarantee that the inetia estimates will be physically admissible ($\boldsymbol{I}$ and $\boldsymbol{A}$ must be positive definite). The convergence of unknown parameters to their true value can only be guaranteed by satisfying the persistence of excitation[27] conditions.

Finally, it should be noted that the analysis presented in this section only assumes that sensor noise is bounded in magnitude, that is, signal-to-noise ratio is bounded. Therefore, this analysis is valid for a large class of measurement errors (systematic or stochastic). Generally, sensor errors are modeled by Gaussian white noise processes and the upper bound on sensor error can be easily related, at least approximately, to a suitably large multiple of the standard deviation of the Gaussian white noise. Regarding the utility of the bounds derived in this paper, we feel that these bounds are useful in selecting appropriate tuning parameters for the controller to achieve desired performance and for selection of measurement sensor characteristics. These criticisms notwithstanding, simulations suggest a strong basis for optimism on the practical value of this formulation and have been fully consistent with the theoretical stability bounds. In summary, the analysis presented in this section allow us, for the first time, to rigorously tie the adaptive controller stability and performance bounds with sensor measurement accuracy bounds.

Numerical Simulations

The control laws presented in this paper are illustrated in this section for a particular rendezvous and docking maneuver. It is assumed that chaser spacecraft is at a distance of $\{-100, -70, -80\}^T$ m from the target spacecraft. The target spacecraft is assumed to be in a circular orbit at an altitude of 400 km. The actual mass of the chaser spacecraft is assumed to be 50 kg with the following true inertia matrix:

$$\boldsymbol{I} = \begin{bmatrix} 250 & 100 & 50 \\ 100 & 200 & 30 \\ 50 & 30 & 150 \end{bmatrix}$$

The chaser is assumed to be equipped with three momentum wheels for attitude control with the following true wheel control influence matrix:

$$\boldsymbol{A} = \begin{bmatrix} 10 & 6 & 5 \\ 6 & 12 & 4 \\ 5 & 4 & 15 \end{bmatrix}$$

For simulation purposes, the position and attitude estimates are assumed to be available at a frequency of 100 Hz, which is generally the case for many relative navigation sensors.[9,10]

Translation Motion

The reference target trajectory for the translation motion of the chaser is generated in a smooth ad hoc fashion by connecting a third-order spline curve between the initial state and the final desired position ($\{0, 0, 0\}^T$ m) of the chaser. To fit the smooth curve, the docking time is assumed to be 10 min. Initial position errors of 1 m are introduced in translation motion components and the initial attitude is set off from the desired one by 50%. Further, the perfect position measurements are corrupted by Gaussian white noise of variance 0.001 m/s$^{1/2}$ to model the sensor noise error. In case of any relative navigation sensor sensor, a truncated Gaussian white noise depicts the nominal geometric state estimation error; note the worst case measurement errors are physically bounded by the sensor field of view. For practical purposes, any simulated noise sample larger than $\pm 4\sigma$ was set to $\pm\sigma$ All the initial conditions and tuning parameters of controller are set as given below:

Translation Motion Initial Conditions:

$$\boldsymbol{x}_1(0) = [-100 \quad -70 \quad -80]^T \text{ m}, \qquad \boldsymbol{z}(0) = [0 \quad 0 \quad 0]^T$$

$$m(0) = 40\,\text{kg}, \qquad \text{an error of } 20\%$$

$$\boldsymbol{A}_m = -\boldsymbol{I}_{3\times 3}, \qquad \boldsymbol{Q} = \boldsymbol{I}_{3\times 3}, \qquad \Gamma_1 = 5$$

Figures 2 and 3 show translation motion position tracking error ($\boldsymbol{e}_1$) and velocity tracking error ($\boldsymbol{e}_2$), respectively. From these plots,

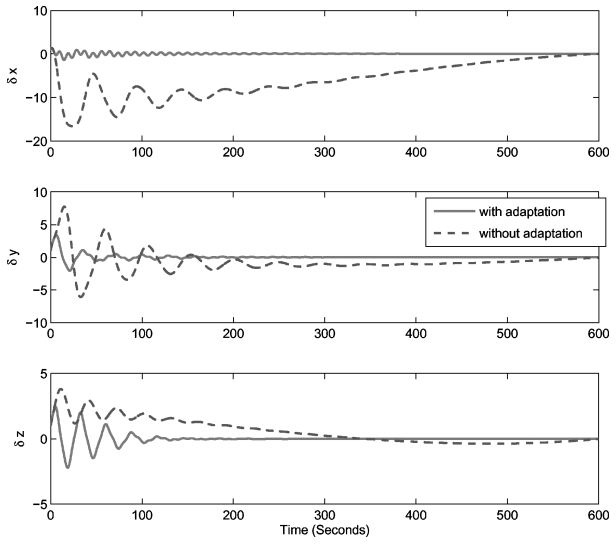

Fig. 2 Position tracking error versus time.

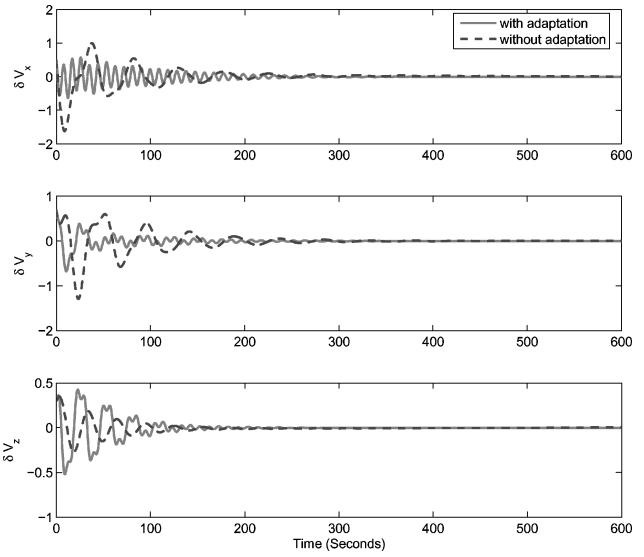

Fig. 3 Velocity tracking error versus time.

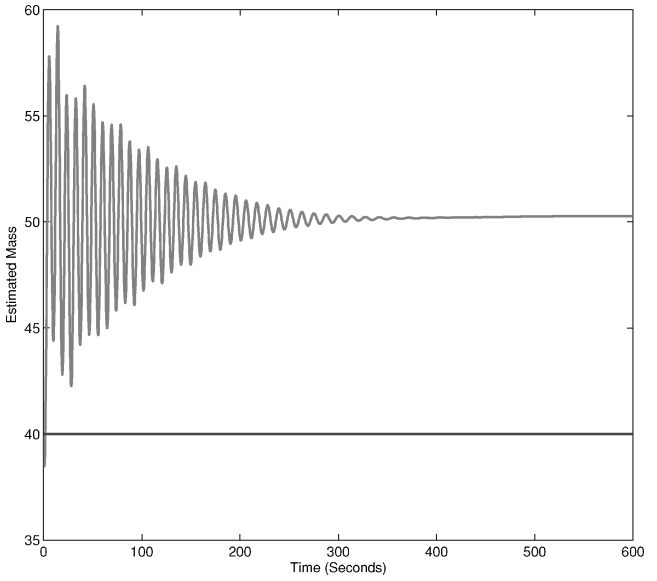

Fig. 4 Estimated mass versus time.

we conclude that the adaptive control law without velocity measurements presented in this paper performs well even in presence of high uncertainty in the mass of the chaser spacecraft. Also, it should be noticed from these plots that velocity tracking error converges faster than position tracking errors, which is consistent with the assumptions made in this paper. The estimated mass of chaser and the corresponding control forces are shown in Figs. 4 and 5, respectively. From Fig. 4, it should be noticed that the estimated mass of the chaser actually converges graphically to its true value. This surprising result, though not guaranteed by the analysis, is pleasing. We infer that the reason for the accurate mass estimate convergence is because of the richness of the translational reference trajectory and that there is only one parameter (spacecraft mass) to learn. Finally, to quantify the effect of measurement noise on the tracking error, the variance of measurement noise is varied from 0.001 m/s$^{1/2}$ to 1 m/s$^{1/2}$. Figure 6 shows the variation of the mean Sobolev norm, $\sqrt{[\boldsymbol{e}_1^T(t)\boldsymbol{e}_1(t) + \boldsymbol{e}_2^T(t)\boldsymbol{e}_2(t)]}$, of the tracking error with the variance of measurement noise while keeping the controller tuning parameters to be same. As expected, the tracking error increases as the variance of measurement noise increases. It should be mentioned that for the particular choice of controller parameters made in this paper, $\dot{V}$ is always negative definite and we faced no problems regarding the divergence of spacecraft mass estimate or tracking error.

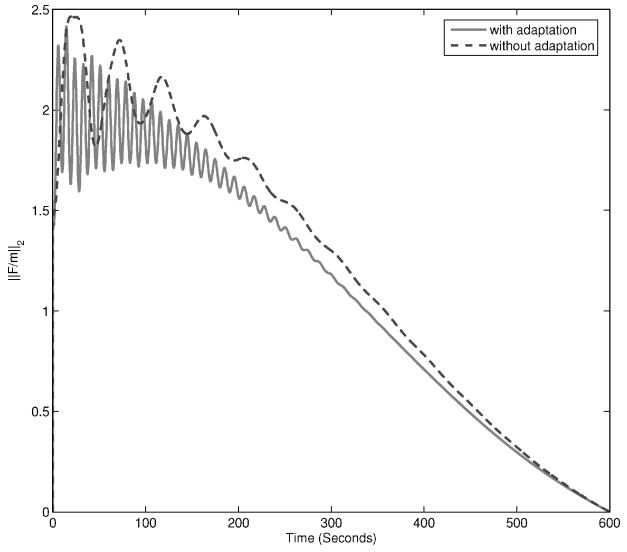

Fig. 5 Required control effort versus time.

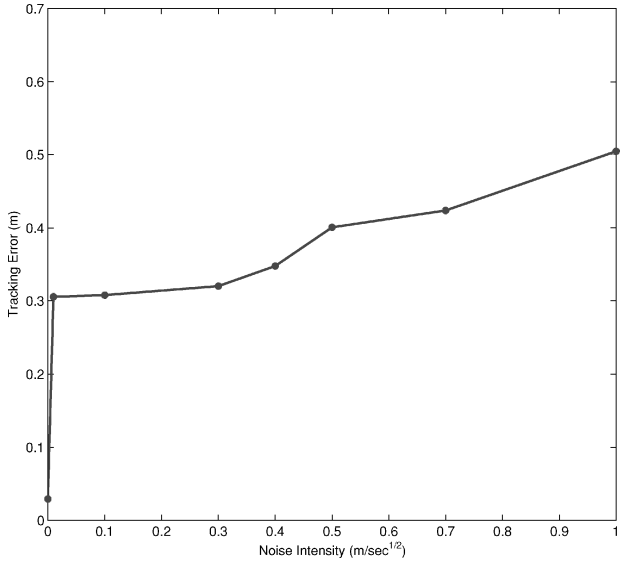

Fig. 6 Tracking error versus noise variance.

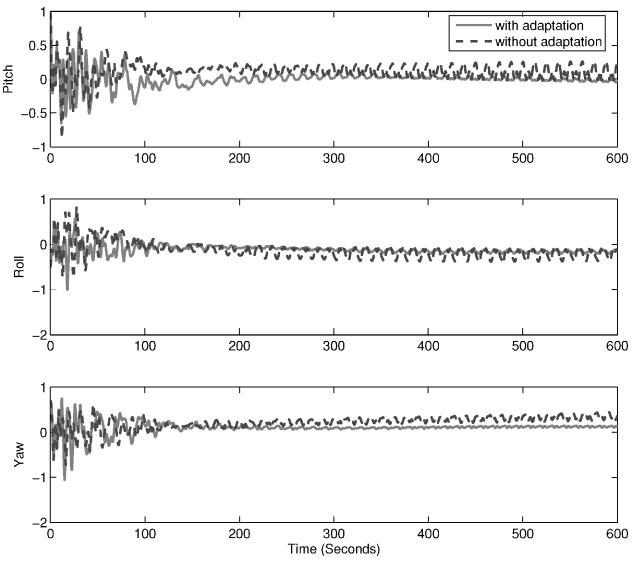

Fig. 7 Attitude tracking error versus time.

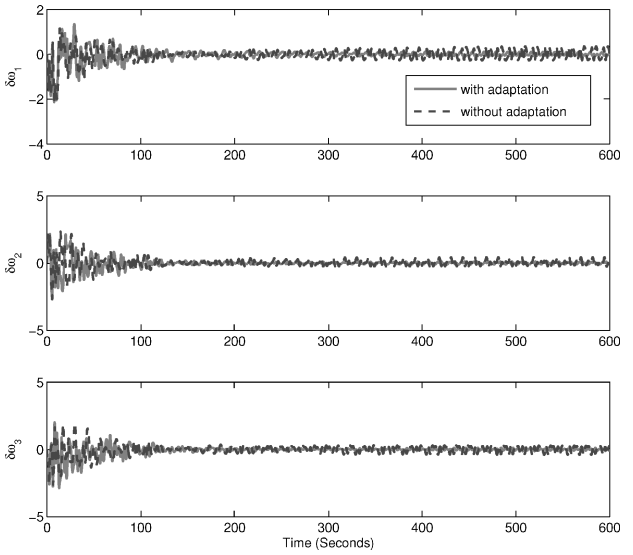

Fig. 8 Angular velocity tracking error versus time.

Rotational Motion

To illustrate the capability of adaptive control law in presence of uncertainties and disturbances, we design a highly demanding attitude maneuver (more difficult than any anticipated "practical" maneuver). The reference attitude trajectory is assumed to be

$$\boldsymbol{\sigma}(t) = \left\{0.5\sin(0.5t) \quad 0.5\sin(0.5t) \quad \sqrt{3}/2\right\}^T \tag{73}$$

Initial attitude errors of $\{1 \ -0.5 \ 0.7\}^T$ are introduced into MRP components. The attitude measurement and momentum wheel velocity measurement errors are modeled by truncated Gaussian white noise of variance 100 μ rad/s$^{1/2}$ and 100 μ rad/s$^{3/2}$, respectively. The initial spacecraft and wheel inertia matrices are perturbed by random variations of variance 20 kg $\cdot$ m^2/s$^{1/2}$ and 10 kg $\cdot$ m^2/s$^{1/2}$, respectively. The various tuning parameters of controller are set as given below:

Rotation Motion Initial Conditions:

We mention that different tuning parameters were selected in such a way that we achieve desired tracking in 10 min. Beside this, we also simulate the effect of the disturbance torque acting on the chaser at frequencies between 2 and 30 Hz. The magnitude of disturbance torque is chosen to be [0.05 0.05 0.01] N $\cdot$ m, whereas initially the magnitude of the disturbance torque is set to zero. Figures 7 and 8 show the attitude tracking error ($\boldsymbol{e}$) and angular velocity tracking error ($\boldsymbol{\delta\omega}$), respectively. The corresponding commanded wheel velocity is shown in Fig. 9. The estimated spacecraft and momentum wheel inertia parameters and unknown disturbance magnitude are shown in Figs. 10–12, respectively. It must be noted that tracking errors in this case are at least two times better when adaptation is on. Once again, as anticipated, velocity-level tracking error converges faster than attitude tracking error. From these results we might anticipate that the control law is capable of handling the disturbance torques due to thruster misalignment, environment, and so forth even in the presence of measurement noise.

$$\boldsymbol{A}_m = -0.05 \times \boldsymbol{I}_{3\times 3}, \qquad \boldsymbol{Q} = 10 \times \boldsymbol{I}_{3\times 3}$$

$$\Gamma_1 = \text{diag}\left\{10^2 \quad 10 \quad 10 \quad 10^2 \quad 10 \quad 10^2 \quad 0.03 \quad 0.03 \quad 0.03 \quad 0.03 \quad 0.03 \quad 0.03 \quad 5 \quad 5 \quad 5\right\}$$

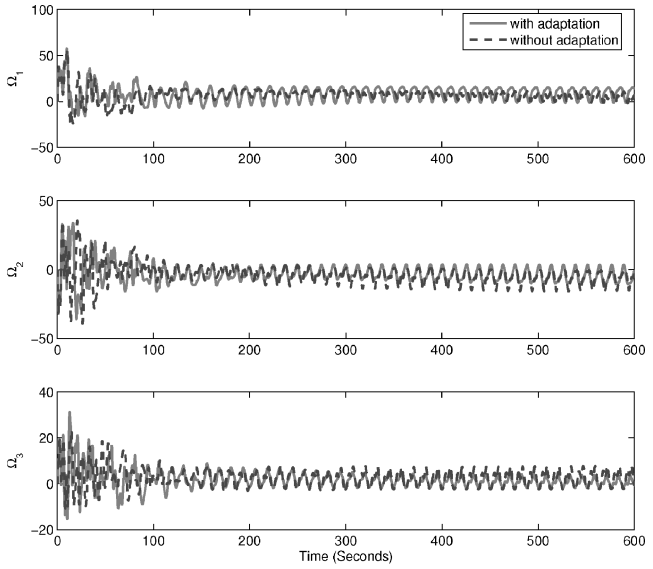

Fig. 9 Commanded wheel velocity (rad/s) versus time.

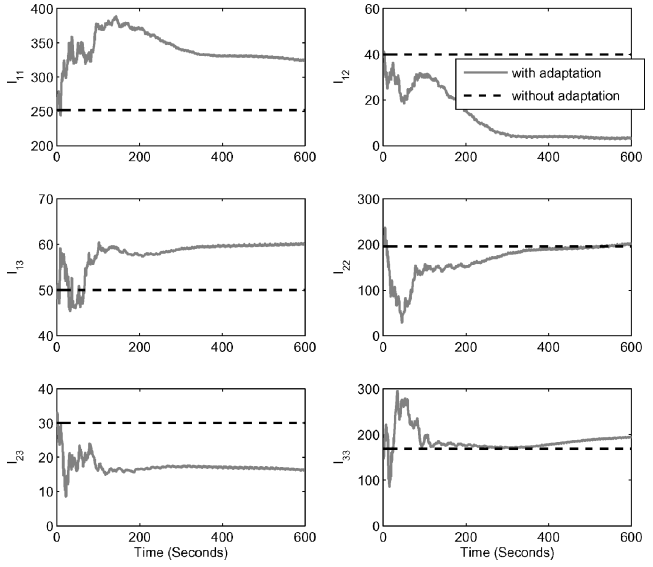

Fig. 10 Estimated spacecraft inertia parameters versus time.

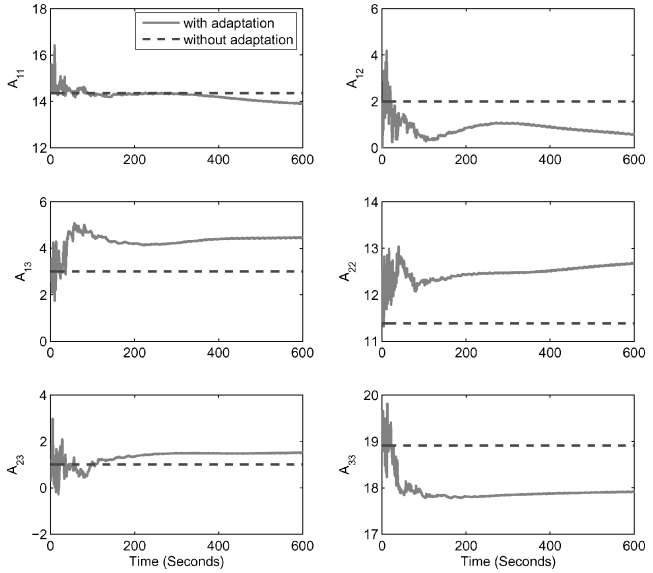

Fig. 11 Estimated wheel inertia parameters versus time.

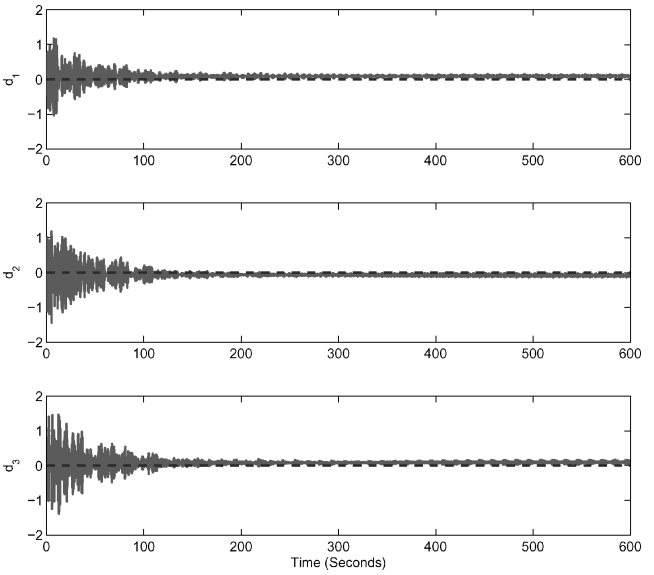

Fig. 12 Estimated disturbance amplitude versus time.

The control effort required in this case can be smoothed further by a more judicious choice of the controller tuning parameters.

Finally, the tuning parameters for the control law were selected by trial and error to illustrate the essential ideas. It is worthwhile to mention that the robustness of the control law depends upon the choice of $\boldsymbol{A}_m$ and $\boldsymbol{Q}$. For large values of $\boldsymbol{Q}$ and small values for $\boldsymbol{A}_m$, we obtain sufficient robustness with respect to uncertainties in the system dynamics and measurement noise. However, this is achieved at the expense of large control effort and lack of smoothness in control and state trajectories.

Conclusions

An asymptotically stable partial state feedback adaptive controller has been designed for spacecraft rendezvous and docking when perfect relative position and attitude measurements are available. The control laws were evaluated against bounded measurement errors in the adaptive control setting. The stability analysis presented in this paper is shown to be valid for a large class of measurement errors (systematic or stochastic). Further, the analysis in the presence of sensor errors lays down a framework to tie together state estimation with controller design for realistic control design purposes. Another key point of the controller design presented in this paper is the accommodation of actuator dynamics uncertainty as momentum wheel inertias were assumed to be unknown. In fact a generalized adaptive control formulation was developed wherein all system mass/inertia properties were considered to be poorly known. This control law was shown to work well in the presence of bounded disturbances, large parameter errors, and measurement noise, fully consistent with the bounded stability analysis presented. Although the simulation results presented in this paper merely illustrate formulations for a particular rendezvous and docking maneuver, further testing would be required to reach any conclusions about the efficacy of the control and adaptation laws for tracking arbitrary maneuvers. In particular, optimization of the remaining parametric degrees of freedom to extremize some measure of performance or robustness should be considered, subject to the stability constraints derived herein.

References

[1]Ambrosius, B. A. C., Hesper, E. T., and Wakker, K. F., "Application of the Global Positioning System for Hermes Rendezvous Navigation," *Journal of Guidance, Control, and Dynamics*, Vol. 16, No. 1, 1993, pp. 197–205.

[2]Wayne, A., Jorge, D., Galdos, I., Upadhyay, T. N., and Lomes, J. J., "GPS Relative Navigation for Automatic Spacraft Rendezvous and Capture," *Proceedings of the National Telesystems Conference*, IEEE Publications, Piscataway, NJ, June 1993, pp. 155–168.

[3]Zimmerman, K. R., and Cannon, R. H., Jr., "Experimental Demonstration of GPS for Rendezvous Between Two Prototype Space Vehicles," *Proceedings of the ION GPS-95 Conference*, Institute of Navigation, Fairfax, VA, Sept. 1995.

[4]Nimelman, M., Tripp, J., Bailak, G., and Bolger, J., "Spaceborne Scanning Lidar System (SSLS)," *Proceedings of SPIE, Spaceborne Sensors II*, Vol. 5798, May 2005, pp. 73–82.

[5]Pelletier, F., Golla, D., and Allen, A., "Lidar-Based Rendezvous Navigation for MSR," AIAA Paper 2004-4987, 2004.

[6]Studor, G., "Laser Dynamic Range Imager Space Shuttle Flight Demonstration," Structural Mechanics Report, NASA JSC, Houston, TX, 1998.

[7]Schmitt, R. L., Williams, R. J., and Matthews, J. D., "High Frequency Scannerless Imaging Laser Radar for Industrial Inspection and Measurement Applications," Sandia Report SAND96-2739, Sandia National Lab., 1996.

[8]Junkins, J. L., Schaub, H., and Hughes, D. C., "Laser Position Sensor," Patent Disclosure Number 017575.0356, cited Sept. 21, 1998.

[9]Junkins, J. L., Hughes, D., Wazni, K. P., and Pariyapong, V., "Vision-Based Navigation for Rendezvous, Docking and Proximity Operations," *Proceedings of the Guidance and Control 1999*, edited by R. D. Culp and D. Wiemer, *Advances in the Astronautical Sciences*, Vol. 101, Univelt, Inc., San Diego, CA, 1999, pp. 203–221.

[10]Katake, A., and Junkins, J. L., "Precision Navigation, Rendezvouz and Docking Using Novel Optical Sensors," *AAS National Conference and 46th Annual Meeting*, Univelt, Inc., San Diego, CA, Nov. 16–18, 1999.

[11]Gunnam, K. K., Hughes, D., Junkins, J. L., and Kehtarnavaz, N., "A VISION Based DSP Embedded Navigation Sensor," *IEEE Sensors Journal*, Vol. 2, No. 5, 2002, pp. 428–442.

[12]Clohessey, W. H., and Wiltshire, R. S., "Terminal Guidance System for Satellite Rendezvous," *Journal of the Aerospace Sciences*, Vol. 27, No. 9, 1960, pp. 653–658.

[13]Subbarao, K., Steinberg, M., and Junkins, J. L., "Structured Adaptive Model Inversion Applied to Tracking Aggressive Aircraft Maneuvers," AIAA Paper 2001-4019, Aug. 2001.

[14]Akella, M. R., "Rigid Body Attitude Tracking Without Angular Velocity Feedback," *Systems and Control Letters*, Vol. 42, No. 4, 2001, pp. 321–326.

[15]Singla, P., "A New Attitude Determination Approach Using Split Field of View Star Camera," Master's Thesis, Texas A&M University, College Station, TX, Aug. 2002.

[16]Singla, P., Crassidis, J. L., and Junkins, J. L., "Spacecraft Angular Rate Estimation Algorithms for Star Tracker-Based Attitude Determination," *Proceddings of the Spaceflight Mechanics 2003*, edited by D. J. Scheeres, M. E. Pittelkau., R. J. Proulx, and L. A. Cangahuala, *Advances in the Astronautical Sciences*, Vol. 114, Univelt, Inc., San Diego, CA, Feb. 2003, pp. 1303–1317.

[17]Crassidis, J. L., "Angular Velocity Determination Directly from Star Tracker Measurements," *AIAA Journal of Guidance, Control, and Dynamics*, Vol. 25, No. 6, 2002, pp. 1165–1168.

[18]Crassidis, J. L., Alonso, R., and Junkins, J. L., "Optimal Attitude and Position Determination from Line-of-Sight Measurements," *Journal of the Astronautical Sciences*, Vol. 48, No. 2, 2000, pp. 391–408.

[19]Mortari, D., Rojas, J. M., and Junkins, J. L., "Attitude and Position Estimation from Vector Observations," *Proceedigns of the Spaceflight Mechanics 2004*, edited by S. L. Coffey, A. P. Mazzoleni, K. K. Luu, and R. A. Glover, *Advances in the Astronautical Sciences*, Vol. 119, Univelt, Inc., San Diego, CA, Feb. 2004, pp. 575–593.

[20]Tsiotras, P., "Further Passivity Results for the Attitude Control Problem," *IEEE Transactions on Automatic Control*, Vol. 43, No. 11, 1998, pp. 1597–1600.

[21]Subbarao, K., and Akella, M. R., "Differentiator-Free Nonlinear Proportional-Integral Controllers for Rigid-Body Attitude Stabilization," *AIAA Journal of Guidance, Control, and Dynamics*, Vol. 27, No. 6, 2004, pp. 1092–1096.

[22]Schaub, H., and Junkins, J. L., *Analytical Mechanics of Space Systems*, AIAA Education Series, AIAA, Reston, VA, 2003.

[23]Singla, P., Subbarao, K., Hughes, D., and Junkins, J. L., "Structured Model Reference Adaptive Control for Vision Based Spacecraft Rendezvous and Docking," *Proceedings of the Spaceflight Mechanics 2003*, edited by D. J. Scheeres, M. E. Pittelkau., R. J. Proulx, and L. A. Cangahuala, *Advances in the Astronautical Sciences*, Vol. 114, Univelt, Inc., San Diego, CA, Feb. 2003, pp. 55–75.

[24]Miwa, H., and Maruthi, M. R., "Global Adaptive Stabilization Using Output Feedback for Spacecraft Attitude Tracking," *Advances in Astronautical Sciences*, Vol. 112, No. 1, 2002, pp. 345–357.

[25]Krstić, M., Kanellakopoulos, I., and Kokotović, P. V., *Nonlinear and Adaptive Control Design*, Adaptive and Learning Systems for Signal Processing, Communications and Control Series, Wiley–Interscience, New York, 1995.

[26]Sastry, S., *Nonlinear Systems: Analysis, Stability and Control*, Springer-Verlag, New York, 1999.

[27]Ionnaou, P. A., and Sun, J., *Robust Adaptive Control*, Prentice–Hall, Upper Saddle River, NJ, 1996.

[28]Tanygin, S., "Generalization of Adaptive Attitude Tracking," AIAA Paper 2002-4833, Aug. 2002.

[29]Cheney, W., *Analysis for Applied Mathematics*, Graduate Texts in Mathematics, Vol. 208, Springer-Verlag, 2000.